3D Super-virtual Refraction Interferometry

Kai Lu, Abdullah AlTheyab and Gerard T. Schuster*
King Abdullah University of Science and Technology

SUMMARY

Super-virtual refraction interferometry enhances the signal-to-noise ratio of far-offset refractions. However, when applied to 3D cases, traditional 2D SVI suffers because the stationary positions of the source-receiver pairs might be any place along the recording plane, not just along a receiver line. Moreover, the effect of enhancing the SNR can be limited because of the limitations in the number of survey lines, irregular line geometries, and azimuthal range of arrivals. We have developed a 3D SVI method to overcome these problems. By integrating along the source or receiver lines, the cross-correlation or the convolution result of a trace pair with the source or receiver at the stationary position can be calculated without the requirement of knowing the stationary locations. In addition, the amplitudes of the cross-correlation and convolution results are largely strengthened by integration, which is helpful to further enhance the SNR. In this paper, both synthetic and field data examples are presented, demonstrating that the super-virtual refractions generated by our method have accurate traveltimes and much improved SNR.

INTRODUCTION

Traveltime tomography is a widely used tool to estimate the subsurface velocity distribution. Unfortunately, the problem with wide-offset refraction surveys is that the head-wave energy at far offsets can be very weak, which leads to a low SNR of first arrivals. In this case, traveltimes of far-offset traces cannot be accurately picked. To overcome this problem, Bharadwaj and Schuster (2010) and Mallinson et al. (2011) developed the theory of super-virtual refraction interferometry to create head-wave arrivals with much improved SNR.

The traditional SVI is only discussed in 2D cases, where all the refractions from the same layer partly share ray paths, and are called stationary. However, in 3D cases, a pair of refraction traces sharing the same source or receiver can not be guaranteed to be stationary because of the freedom given by the additional dimension in space. In another aspect, the number of source and receiver pairs used to generate a particular head wave, which determines the improvement of the SNR, can be very few when the source and receiver of the targeted trace are at neighboring survey lines. Therefore, applying traditional SVI on 3D cases can be problematic.

This paper proposes a modified 3D SVI method, combining the 2D SVI method with stationary phase integration. Analogous to the application of stationary phase integration on interferometric redatuming (Snieder, 2004), we calculate the cross-correlation or convolution of the stationary trace pair by integrating over the sources and receivers along the survey lines, without the requirement of knowing the locations of stationary sources or receivers. Moreover, this additional integration step also contributes to enhancing the SNR, and thus helps to partly overcome the problems caused by the limitations of the survey geometry.

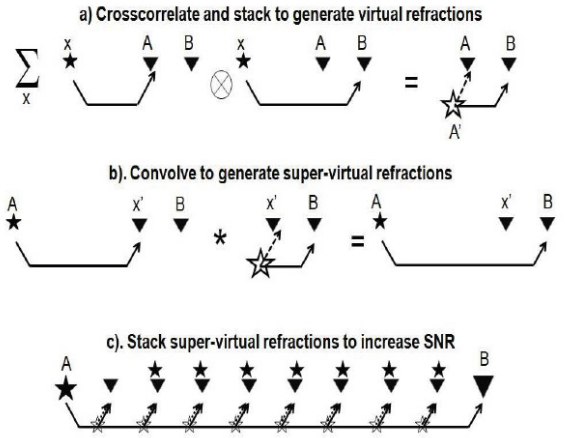

Figure 1: The steps for creating 2D super-virtual refraction arrivals. *a*. Correlation of the recorded trace at A with that at B for a source at x to give the trace $\phi_x(A,B,t)$ with the virtual refraction having traveltime denoted by $\tau_{A'B} - \tau_{A'A}$. This arrival time will be the same for all post-critical source positions, so stacking $\sum_x \phi_x(A,B,t)$ will enhance the SNR of the virtual refraction by $\sqrt{N}$. *b*. Similar to that in a) except the virtual refraction traces are convolved with the actual refraction traces and stacked for different geophone positions to give the *c*. Super-virtual trace with a SNR enhanced by $\sqrt{N}$. Here, N denotes the number of coincident source and receiver positions that are at post-critical offset.

THEORY

The far-field reciprocity equation of both correlation and convolution types are used to construct super-virtual refractions (Bharadwaj et al., 2011). Figure 1 describes the conventional procedure for creating super-virtual refractions in far-offset traces.

The assumption is that all the refractions partly share common ray paths, which is guaranteed in 2D cases. In 3D cases, in order to apply the SVI scheme directly, the trajectory along which all the sources and receivers are stationary is required. However, the locations of stationary sources and receivers are unknown and difficult to find in practice.

To avoid the difficult task of locating the stationary sources and receivers, we calculate the cross-correlation or convolution of a stationary trace pair indirectly by applying stationary phase integration (Schuster, 2009) to the source and receiver lines.

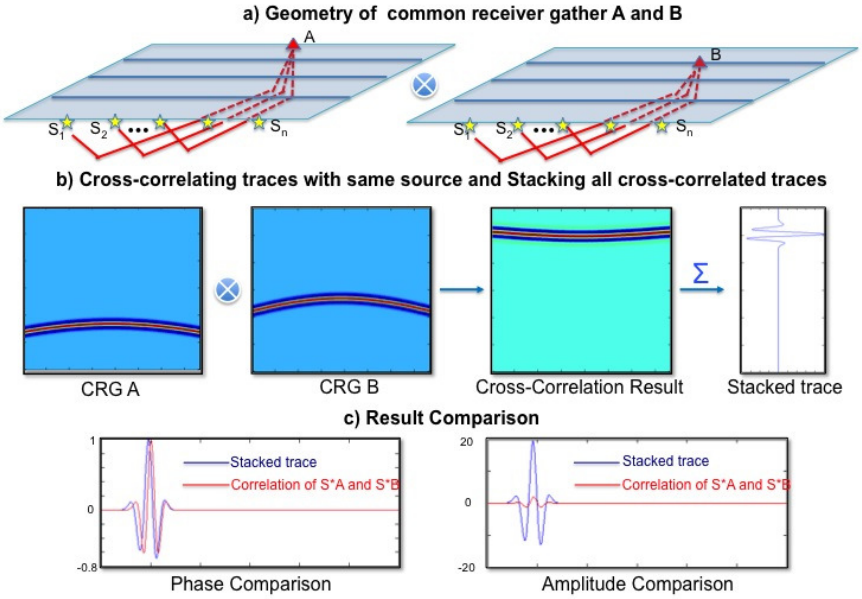

Figure 2: Illustration for creating a virtual trace in 3D with stationary phase integration. a) The geometry of receivers A and B, and the selected source line for integration. b) CRG A and CRG B show the refractions from the same horizontal layer. Every trace in CRG A is cross-correlated with the trace sharing the same source in CRG B. c) All the traces after cross-correlation are stacked to generate the virtual trace AB. The virtual trace generated by integration is compared with that generated by cross-correlating refraction S^*A and S^*B, where S^* is the stationary source location. The stacked virtual trace has an accurate traveltime and much strengthened amplitude.

The stationary phase analysis (Bleistein, 1984) is applied to the line integral:

$$f(\omega) = \int_{-\infty}^{\infty} g(x) e^{i\omega\phi(x)} dx \sim \alpha e^{i\omega\phi(x^*)} g(x^*), \qquad (1)$$

where $\phi(x)$ is real and a well-behaved phase function with at most one simple stationary point, ω is the asymptotic frequency, and $g(x)$ is a relatively slowly varying function, $\alpha = e^{i\pi/4}\sqrt{2\pi/(\omega|\phi(x^*)|)''}$ is an asymptotic coefficient, and $x = x^*$ is a stationary point.

Figure 2 illustrates how stationary phase integration can be applied to the correlation-reciprocity type in SVI. Let $G(A|S) = e^{i\omega\tau_{SA}}$ and $G(B|S) = e^{i\omega\tau_{SB}}$ approximate the normalized refraction wave as shown in Figure 2(a), then Equation 1 becomes

$$\int_{S_1}^{S_n} G(A|S) G^*(B|S) dS \sim \alpha_1 e^{i\omega(\tau_{S^*A} - \tau_{S^*B})}, \qquad (2)$$

where S^* denotes the stationary point, α_1 is a coefficient, and far-field approximation is assumed. The left-hand side in Equation 2 is the summation of cross-correlation results along the source line, and the right-hand side represents the virtual refraction AB multiplied by a coefficient. It means that we can calculate the virtual traces by integrating along the source line without knowing the exact location of the stationary point. By comparing the integration result with the virtual trace AB generated by cross-correlating refraction S^*A and S^*B, we can see that the phase matches well. Moreover, the amplitude is enhanced by stationary phase integration, which can further contribute to improving the SNR. This is helpful in the cases where the source and the receiver are on lines near to each other,and there are a limited number of sources and receivers available for SVI. Noticing that Equation 2 is not dependent on which source line we select for integration, and the result can be the same if we choose different source lines, we repeat the above procedures using several source lines, and stack all the virtual traces generated, as shown in Figure 3(a), to improve the SNR. The idea in this step is similar with stacking virtual traces associated with different sources x in traditional 2D SVI as shown in Figure 1(a).

In a similar way, stationary phase integration can be applied to the convolution-reciprocity integral used with SVI. Let $G(A|B)^{virt} = e^{i\omega(\tau_{S(B)A} - \tau_{S(B)B})}$ denote the normalized virtual traces calculated in the previous step, where $S(B)$ is the stationary source location associated with a specific receiver B, and apply Equation 1 along the receiver line,

$$\int_{B_1}^{B_n} G(B|S) G(A|B)^{virt} dB \sim \alpha_2 e^{i\omega(\tau_{SB^*} + \tau_{S(B^*)A} - \tau_{S(B^*)B^*})}, \qquad (3)$$

where B^* is the stationary receiver location associated with the given source S and receiver A, and α_2 is the coefficient. Recognizing that $S(B^*)$ is actually the given source S in Figure 3(b), Equation 3 becomes

$$\int_{B_1}^{B_n} G(B|S) G(A|B)^{virt} dB \sim \alpha_2 e^{i\omega\tau_{SA}}. \qquad (4)$$

The left-hand side of Equation 4 is the summation of the convolution results along the receiver line, and the right-hand side

represents the super-virtual refraction SA multiplied by a coefficient. Figure 3(b) illustrates the step of stacking super-virtual traces generated with different receiver lines.

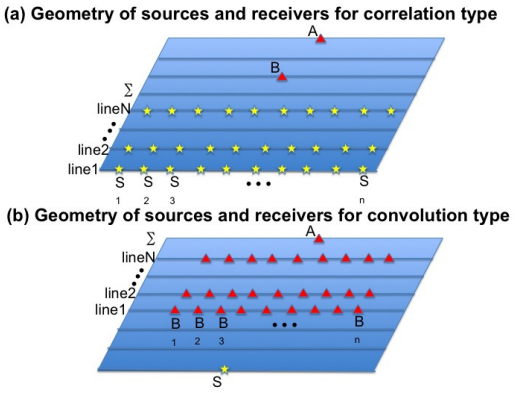

Figure 3: The geometry of sources and receivers for correlation type and convolution type. (a) Virtual traces AB generated with different source lines from line1 to line*N* are stacked. (b) Super-virtual traces SA generated with different receiver lines from line1 to line*N* are stacked.

Below is the workflow for 3D super-virtual refraction interferometry:

1. Filter the raw data to remove high-frequency noise.
2. Choose a proper window size for the target refraction.
3. Generate the stationary virtual traces by cross-correlation and integrate along a source line.
4. Stack the virtual traces generated from different source lines as shown in Figure 3(a).
5. Generate the stationary super-virtual traces by convolution and integrating along a receiver line.
6. Stack the super-virtual traces generated from different receiver lines as shown in Figure 3(b).

NUMERICAL RESULTS

Synthetic Data Test

Synthetic data are tested to demonstrate the effectiveness of the proposed method. Figure 4 shows the 3D velocity model with an undulating layer and the geometry with 11 survey lines on the ground, and 76 shots and 301 receivers in each line.

A common shot gather is shown in Figure 5(a), with the source located at the leftmost of Line1, and the receivers at Line11. The first arrivals of the far-offset traces are impossible to pick after strong random noise being added to the synthetic data as shown in Figure 5(b). 3D SVI are applied to the noisy data, and the super-virtual data are shown in 5(c). The far-offset traces have stronger amplitude and more improved SNR, which is because refractions do not exist when the source and the receiver is too close in the near offset, and thus fewer traces are stacked. The more amplitude-balanced data are shown in Figure 5(d) after trace-by-trace normalization. Compared to the input shown in Figure 5(b), the final SVI output shown in Figure 5(d) has the correct traveltimes and much improved SNR. In addition, traditional 2D SVI will suffer with such a narrow geometry with only 11 survey lines because of the limited sources and receivers available for stacking, while we overcome this problem with the contribution from the stationary phase integration to further enhance the SNR.

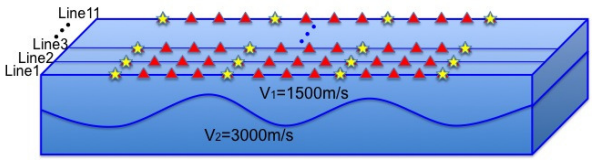

Figure 4: The undulating layer velocity model for synthetic test. 11 survey lines are placed on the ground, with 76 sources and 301 receivers in each line.

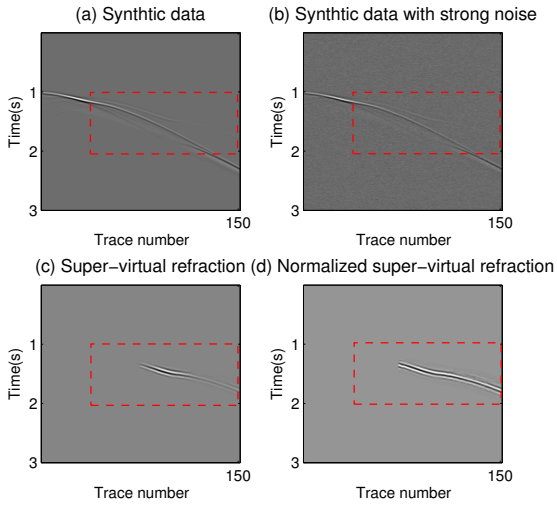

Figure 5: a) The raw common shot gather. b) Strong random noise is added to (a). c) The super-virtual refraction. d) Trace normalized super-virtual refraction.

Field Data Test

In this section, the proposed method is applied to a 3D OBS field data set recorded in the Gulf of Mexico. The survey geometry is shown in Figure 7. The black dots represent recorders installed at the ocean bottom with the depth about 45 m. There are in total 9 OBS lines, and 26 stations in every line with a spacing of approximately 400 m. The green lines represent 153 sail lines, and 360 shots are excited along every sail line with a shot interval of 50 m. We extract a common OBS gather associated with one sail line from the whole data as an example here. The location of the specific OBS station is at the red star and the sources are at the red line marked in Figure 7. Four OBS lines and 11 sail lines are selected for stationary phase integration schemes.

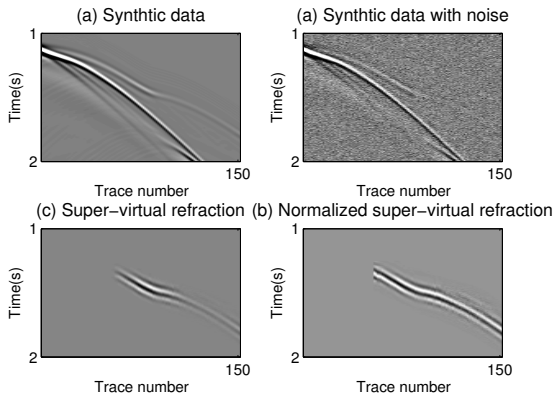

Figure 6: Zoom views of red boxes in Figure 5.

For the convenience in windowing a specific refraction, a 5-15 Hz band-pass filter is applied to suppress the high-frequency noise. Figure 8(a) shows a field data after band-pass filtering. The two events pointed by the red arrows are the target refractions to be processed. We apply 3D SVI to each refraction separately, the results are normalized trace by trace and plotted together as shown in Figure 8(b). We compare the super-virtual data with the band-pass filtered data by a zoom view as shown in Figure 9. The result shows that the super-virtual traces have much improved SNR compared to that of both the raw and band-pass filtered data. Red-lines are plotted at the same locations of both the zoom views in order to check the accuracy of the super-virtual traces. It is clear that the travel-times of the super-virtual traces are acceptably accurate.

To further improve the SNR of the data, either iterative SVI (Al-Hagan et al., 2011) or selecting more source and receiver lines for integration can be used. However, the cost is greater CPU resources and computation time.

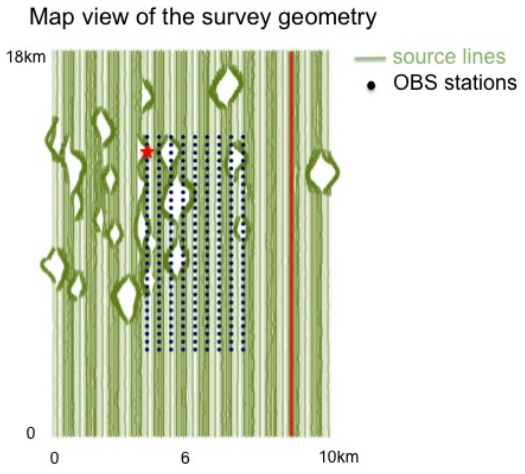

Figure 7: The map view of the survey geometry. The data example shown in the following is an OBS gather with the OBS station located at the red star, and the receivers located at the red line.

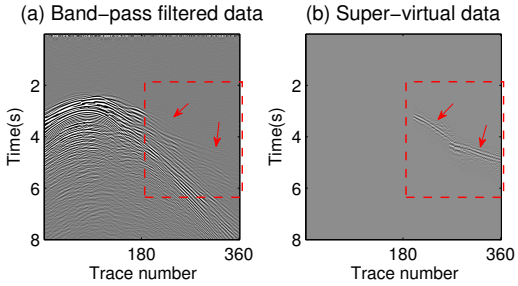

Figure 8: Field data example. (a) 5-15Hz band-pass filtered data (b) The super-virtual data with two refractions.

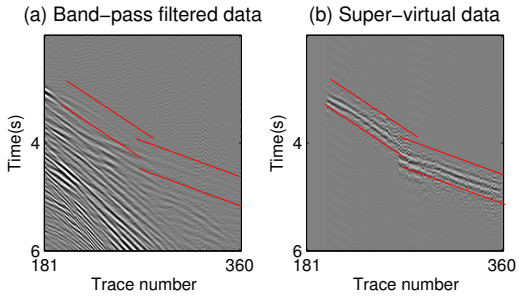

Figure 9: Zoom views of the red boxes in Figure 8 of (a) the band-pass filtered data and (b) the super-virtual data.

DISCUSSION AND CONCLUSION

We introduced the general theory of 3D super-virtual interferometry. A stationary phase integration method is applied with the benefits of avoiding locating the stationary sources and receivers, and further enhancing the signal-to-noise ratio. Both synthetic and field data examples are presented to demonstrate the effectiveness of this method. The most significant drawback of this method is that artifacts can be produced because of the limited aperture for integration as well as a coarse spacing of sources or receivers. Our future work is to test how much percentage of the pickable range can be increased by SVI for the whole 3D dataset, and to explore how much improvement can be achieved in 3D traveltime tomography with the benefits of the additional traveltime picks.

ACKNOWLEDGMENTS

We thank the CSIM members for supporting this research, and we also thank the High Performance Computational Center and IT support at KAUST.